



TITLE:

Meso- $\gamma$ -scale convective systems observed by a 443-MHz wind-profiling radar with RASS in the Okinawa subtropical region

AUTHOR(S):

Mikami, Aya; Kawabata, Takuya; Satoh, Shinsuke; Furumoto, Jun-Ichi; Nagai, Seiji; Murayama, Yasuhiro; Tsuda, Toshitaka

---

CITATION:

Mikami, Aya ...[et al]. Meso- $\gamma$ -scale convective systems observed by a 443-MHz wind-profiling radar with RASS in the Okinawa subtropical region. *Journal of Atmospheric and Solar-Terrestrial Physics* 2011, 73(9): 996-1009

ISSUE DATE:

2011-06

URL:

<http://hdl.handle.net/2433/141849>

RIGHT:

© 2010 Elsevier Ltd.; 10.1016/j.jastp.2015.08.012; この論文は出版社版ではありません。引用の際には出版社版をご確認ご利用ください。; This is not the published version. Please cite only the published version.

Meso-  $\gamma$  -scale convective systems observed by a 443-MHz wind-profiling  
radar with RASS in the Okinawa subtropical region

Aya Mikami<sup>(1) #</sup>, Takuya Kawabata<sup>(2)</sup>, Shinsuke Satoh<sup>(3)</sup>, Jun-ichi Furumoto<sup>(1)</sup>,  
Seiji Nagai<sup>(3)</sup>, Yasuhiro Murayama<sup>(3)</sup>, and Toshitaka Tsuda<sup>(1)</sup>

(1) Research Institute for Sustainable Humanosphere (RISH), Kyoto University

(2) Meteorological Research Institute (MRI), Japan Meteorological Agency (JMA)

(3) National Institute of Information and Communications Technology (NICT)

# Now at Osaka Gas Co. Ltd.

Corresponding author: Toshitaka Tsuda

29 May 2010

## Abstract

We observed a meso- $\gamma$ -scale convective system in July 2007 using a 443-MHz wind profiler radar (WPR) with a radio acoustic sounding system (RASS) at the NICT Ogimi observatory in Okinawa, Japan. We analyzed the virtual temperature,  $T_v$ , the Brunt-Vaisala frequency squared,  $N^2$ , and three components of the profiles of wind velocities from the WPR-RASS data. We also employed a non-hydrostatic meso-scale (NHM) numerical model. Although the island of Okinawa was covered with a Pacific high-pressure system from 21-26 July, it was convectively unstable below about 5 km. A number of convective clouds generally appeared from 11:00-18:00 in local time (i.e., Japan Standard Time; JST) with a typical horizontal scale of 10 km and temporal scale of 40 - 60 minutes. We focused on the convective system that passed over the Ogimi radar site on 23 and 25 July. Just before rain occurred on these days, a low  $N^2$  region extended upward to 2.0 km, which is also commonly seen around a convective cloud in the NHM model. The cloud water content from the NHM model indicated that the cloud top height correlates with the low  $N^2$  structure. Before the convective system was generated,  $N^2$  decreased below an altitude of about 1 km altitude, because air with low  $T_v$  intruded at 1-3 km, and the surface temperature increased due to solar radiation. The sea-breeze from both the east and west coasts of Okinawa collided to force the convergence below 1 km. Thus, the synergetic effects of the low static stability and convergence seemed to trigger the generation of a convective system, which eventually grew up to 11 km over the radar site.

KEY WORDS: wind profiler, RASS, NHM model, meso-scale convection

1  
2  
3  
4  
5  
6  
7  
8  
9  
10  
11  
12  
13  
14  
15  
16  
17  
18  
19  
20  
21  
22  
23  
24  
25  
26  
27  
28  
29  
30  
31  
32  
33  
34  
35  
36  
37  
38  
39  
40  
41  
42  
43  
44  
45  
46  
47  
48  
49  
50  
51  
52  
53  
54  
55  
56  
57  
58  
59  
60  
61  
62  
63  
64  
65



## 1. Introduction

A meso-scale convective system is characterized by precipitation consisting of both convective and stratiform regions on various horizontal scales. Ninomiya and Akiyama [1992] clarified the hierarchic structure of multiple scales of the precipitation system, and found that a cloud cluster has a structure ranging from meso- $\alpha$  (1,000 km) to meso- $\beta$  (several 100 km) and meso- $\gamma$  (several km) scales. Further, the interaction between two or more scales plays an important role in the development and maintenance of a precipitation system. Within a meso- $\gamma$ -scale convection, there are individual cumulonimbus clouds (convective cells) with the scale even smaller than the meso- $\gamma$ -scale, and convective cells are the important elements that result in a heavy rain.

A number of studies were conducted about generation of convection over a flat terrain. For example, Kobayashi et al. [2004] studied an isolated cumulonimbus cloud developed under high temperature and high pressure in summer over the Kanto Plain of Japan. The key generating factor was investigated by using a Doppler sodar, and they found the importance of a shear line (a localized front) of wind due to a thermal low formed by surface heating. Convergence in the lower layer by a penetrating sea breeze was also important in generating cumulonimbus clouds.

Sea breeze circulation during the daytime usually forms the convergence of low-level wind at the leading edge, which is referred to as a sea breeze front. Cumulonimbus clouds may occur in the convergence region in association with a sea breeze front [e.g. Nicholls et al., 1991; Pielke, 1991]. Using three-dimensional numerical simulation, Pielke [1974] found that location of thunderstorms along the east coast of Florida was controlled by the location and motion of a sea

breeze. From observational studies in Florida, Wakimoto and Atkins [1994] and Atkins and Wakimoto [1995] found that clouds were developed in an area where an updraft of horizontal convective rolls merged with an updraft caused by a sea breeze front. The sea breeze circulation over the island of Java in Indonesia was also studied by Hadi et al. [2001].

The Florida Peninsula and the island of Java are more than 50-200 km wide, while the island of Okinawa is rather narrow ranging from 4 km to 20 km. We focused on the relation between sea-breeze circulation and convective clouds over a small island, like Okinawa. An observation campaign, named the Maritime Continent Thunderstorm Experiment (MCTEX), was conducted around the Tiwi Island in Northern Australia in 1995 [Keenan et al., 2000]. Extensive analyses were conducted from MCTEX in order to clarify the behavior of thunderstorms over tropical islands, focusing on their interactions with the sea breeze [Carbone et al., 2000; Wilson et al., 2001]. By using the MCTEX results with a windprofiler radar (WPR), radio acoustic sounding system (RASS) and a polarimetric radar, the dynamical and thermal structure of tropical storms and the evolution of island boundary layers have been studied [e.g., May, 1999; Schafer et al., 2001].

As Okinawa is situated under a subtropical oceanic region in a warm ocean current (Kuroshio), its climate is characterized by high temperature and high humidity throughout the year. Disturbed meteorological conditions around Okinawa have been studied in terms of typhoons and Baiu fronts. In addition to these studies, meso-scale convective systems over Okinawa under relatively quiet conditions have also been studied. For example, Akaeda et al. [1991] and Chang and Yoshizaki [1991] investigated meso- $\beta$ -scale convective systems when the island of Okinawa was covered with a high-pressure system. Akaeda et al. [1991] found an evolution process and a fine structure during the formative to mature stages of a meso- $\beta$ -scale convective system from Doppler

radar observations at Naha in June 1987. In the formative stage, convective scale updrafts and downdrafts were the predominant flow features, and in the mature stage, a meso-scale flow became dominant, similar to a squall line in the tropics and mid-latitudes. They also clarified that the convective system was stationary at the formative stage and it began to move in the mature stage.

Chang and Yoshizaki [1991] carried out a two-dimensional numerical simulation on the convective system reported by Akaeda et al. [1991], and found that the convection occurred on the leeward side of mountains, indicating that mountain wave were the key factors generating a convective system. For the movement of convection, they also found that the stationary stage of a convective system was established when the formation of a cloud dome was blocked by a mountain. Once cold air flows over a mountain, the system rapidly moves windward.

This paper is concerned with a case study on a meso-scale convective system over the island of Okinawa with a scale smaller than those used in earlier studies. We focused on a convective system on 23 and 25 July 2007 when the area was covered by a Pacific high-pressure system, and studied generation and development processes of the meso- $\gamma$ -scale convective system. We used observations of wind velocity and virtual temperature obtained from a 443MHz WPR with RASS, as well as the data observed with NICT's C-band polarimetric radar (COBRA) and results from a non-hydrostatic meso-scale (NHM) model results. We particularly analyzed atmospheric stability obtained from continuous temperature data with RASS, which plays an important role in the generation of a convective system.

## 2. Radar Data and NHM Model

The 443MHz WPR is installed at the NICT Ogimi observatory (26.68°N, 128.16°E, 225 m

MSL) in Okinawa [Adachi, 2002]. It is also operated as part of the Wind Profiler Network and Data Acquisition System (WINDAS) of JMA. The three components of wind velocity are obtained every 4 minutes with a height resolution of 150 m. The RASS technique was applied to the MU radar by Matuura et al. [1986] in order to obtain temperature profiles simultaneously with the three components of wind velocity. Then, RASS has been widely adopted for WPR on VHF and UHF bands, including an operational WPR network of NOAA [Martner et al. 1993]. We applied RASS to the 443MHz WPR to measure the virtual temperature profile from an altitude of 400 m to 4 km.

We also referred to the data from COBRA [Nakagawa et al., 2002; 2003], which is operated at the Nago observatory located 14 km southwest of the 443MHz WPR site. In July 2007 COBRA was operated in the plan position indicator (PPI) mode at 14 elevation angles and in the range height indicator (RHI) mode every six minutes to obtain a three-dimensional structure of rainfall. We used the reflective intensity (reflectivity) and the Doppler velocity.

We employed an NHM model which is used for an operational weather forecasting at JMA. Details on the NHM model have been described by Saito et al. [2006]. First, we conducted numerical experiments on the NHM model with a grid size of 5 km, assuming the initial and lateral boundary conditions on 23 and 25 July 2007 from the six hourly operational meso-scale analysis at JMA. Then, a down-scaling experiment with a 1-km grid spacing was carried out. The initial state of the simulation was defined at 10:00 JST (01:00 UTC) and the forecast was calculated for six hours. A stretched grid was employed for the vertical axis to increase the vertical resolution at the lower layer; the smallest/largest grid interval was 40 m/1,120 m (2 hPa/104hPa), respectively. The results with the 1-km grid spacing were used in this study, and there were 244x244 horizontal grids. The prognostic variables used in this study were height,  $h$ , temperature,  $T$ , specific humidity,  $q$ ,

three dimensional wind velocities  $u$ ,  $v$ , and  $w$ , integrated precipitation rate and cloud water content (CWC).

### 3. Basic Characteristics of Meso- $\gamma$ -scale Convective System in July 2007 over Okinawa

#### 3.1 Operational Radiosonde and Weather Radar Results

In July 2007, a Baiu-front existed over the mainland of Japan extending from Tohoku to northern Kyushu, but, the island of Okinawa was covered by a Pacific high-pressure system throughout 21-26 July 2007 with its center located south of Okinawa. Although the synoptic-scale condition was not generally disturbed, convective clouds occasionally developed over the island of Okinawa.

The equivalent potential temperature,  $\theta_e$  in Fig. 1 was calculated from 21 to 26 July from 12-hourly routine balloon observations at the Naha weather station (26.12N, 127.41E), located 109 km southwest from the Ogimi observatory. A layer with  $\theta_e > 350$  K, consisting of warm and moist air, was continuously identified below about 0.5-1 km. The small  $\theta_e (< 334$  K, light shaded area in Fig. 1) appeared in two height regions at about 4 and 5 km from 21 to 22 July, and it persisted at around 5.0 km from 23 to 25 July. After 25 July the layer moved downward to an extent such that the lower edge ( $=334$  K) was seen at 4 km, and it further descended to 2.5 km on 27 July. The height range below the region shaded light grey can be considered to be convectively unstable.

We investigated the horizontal distribution of the precipitation rate from the operational weather radar of JMA (the results on 25 July are plotted in Fig. 2). On 21 and 22 July, a weak rain cloud, with a precipitation rate of less than 1.0 mm/hr, was generated in the morning (06:00-11:00

JST) in the southern area of Okinawa near Naha. However, no further development of a cloud system was identified, and the cloud disappeared in the afternoon. From 23 to 25 July, a weak rain cloud also appeared in the morning in the southern area of Okinawa Island similar to the case on 21 or 22 July. The convective cloud activity did not stop, and it also continued throughout the afternoon with a precipitation rate of more than 30.0 mm/hr. Strong convective clouds were identified at many locations all over the island of Okinawa, with a typical horizontal scale of 10 km and a temporal scale of 40 - 60 minutes. On 23 and 25 July, a developed cloud passed through the Ogimi radar site located in northern Okinawa. In each case, the rain cloud disappeared at night after 19:00 JST. On 26 July, no rain clouds appeared throughout Okinawa.

The operational radar results on 25 July are plotted in Fig. 2. A weak rain cloud with a precipitation rate of less than 1.0 mm/hr was first generated only near Naha (near the south end of the Okinawa island) in the morning, then, a number of convective systems were generated from 12:40 to 18:00 JST all over the island. From these cloud systems, precipitation up to 4.5 mm/10min was measured with a tipping-bucket rain gauge at the Ogimi site from 15:30 – 17:40 JST. We estimated the lifting condensation level (LCL), level of free convection (LFC), convective available potential energy (CAPE), and convective inhibition (CIN) for the surface parcel using NHM model data. As the LCL was 315.3 m and the LFC was 1237.5 m, and the CAPE was 1202.4 J/kg and the CIN was 3.2J/kg at the Ogimi WPR site, the environment could easily induce convection.

The meteorological conditions on 23 July were similar to those on 25 July. The operational radar results (not illustrated) revealed that there was a weak convective cloud existed around Naha only from 07:00 – 10:50 JST, and a convective system of more than 30.0 mm/hr, having a horizontal scale of 10 km and a temporal of 40 - 60 minutes, was generated from 11:00 –

17:30 JST over some locations. Of these, precipitation of up to 7.0 mm/10 min from 13:30 – 14:50 JST was measured with a surface rain gauge at Ogimi. The LCL was 194.4 m and the LFC was 1110.0 m, and the CAPE was 1245.2 J/kg and CIN was 2.0J/kg.

These two cases on 23 and 25 July had an overall similarity. That is, a weak convective cloud first occurred in southern Okinawa during the morning, many convective systems were generated all over Okinawa from midday, and they all disappeared by late evening. Such developments and dissipation cycles of the convective system were very similar on both days. However, convection on 23 July started earlier and developed stronger than that on July 25.

Figure 3 shows rainfall intensity from the NHM forecast on 25 July. Note that no significant convective systems were recognized in the NHM model at Ogimi on 25 July. (Situation was similar on 23 July as well, although the plots are not shown.) It was therefore difficult to make a direct comparison between the model and observation at Ogimi. Hence, we surveyed a convective system in the NHM results that demonstrated similar precipitation characteristics to the case observed at Ogimi on 23 and 25 July. On 25 July, the NHM model predicted a strong convective system in the area surrounding Nago, located about 15 km southwest of Ogimi (cross symbol in Fig. 3). In later sections we will compare the model results near Nago with the WPR-RASS observations at Ogimi.

### 3.2 Static Stability Structure Around a Convective System

Taking advantages of the continuous temperature measurements with RASS, we investigated variations in the detailed time-height structure of atmospheric stability during the generation and development of a convective system. It is known that the static stability of moist but

unsaturated air is proportional to the vertical gradient of  $T_v$  [e.g., Emanuel, 1994]. Consequently, we analyzed  $N^2$  every four minutes using the  $T_v$  profiles observed with the 443MHz WPR-RASS on 23 and 25 July over the Ogimi site. We also referred to  $N^2$  from the NHM model results to be able to discuss the general relation between the stability and the convective system. We first present such event from the NHM results with and without convective clouds. Then, we compare them with the observed convective system at Ogimi in terms of the structure of static stability and its relation to the generation of a convective system.

Figure 4 shows the time-height distribution of  $N^2$  near Nago where a convective system appeared in the NHM simulation. (Note that this can be considered as a representative case of a convective system in the model.) The NHM model simulated rain from 14:55-15:35 JST. The model showed the  $N^2$  structure in a height range below 1.2 km where WPR-RASS data was not available, and we found a negative  $N^2$  ( $-0.73 \times 10^{-4} \text{ rad/s}^2$ ) below about 0.8 km that persisted from 10:00 JST until 14:30 JST. That is, the atmosphere was statically unstable near the ground. However, at 1.2-2.2 km, the  $N^2$  was as large as  $1.5\text{-}2.2 \times 10^{-4} \text{ rad/s}^2$ , indicating that this layer was statically stable. That is, a stable layer was laid over a statically unstable layer. However, the  $N^2$  at 1.2 km rapidly decreased from  $1.71 \times 10^{-4} \text{ rad/s}^2$  to  $0.93 \times 10^{-4} \text{ rad/s}^2$  from 14:20-14:30 JST. Then, a low static stability region abruptly moved toward higher altitudes. We will show later that such distinct behavior in the static stability of the model agrees well with the observed  $N^2$  structure on both 25 and 23 July.

We also investigated a case without convection in Fig. 5. As can be seen from Fig. 5, there existed a layer with negative  $N^2$  ( $-0.41 \times 10^{-4} \text{ rad/s}^2$ ) below about 0.7 km before 12:30 JST, the layer near the ground was statically unstable, while, at 1.0-1.8 km,  $N^2$  was  $1.5\text{-}2.2 \times 10^{-4} \text{ rad/s}^2$ , indicating



static stability. In Fig. 5 we noticed very little development of a low stability region with upward motion, although the layer structure might look similar to the one observed in Fig. 4 (with convection).

Figures 6 and 7 show the time-height distribution of the (virtual) potential temperature,  $N^2$  observed with RASS on 25 July and 23 July, respectively, together with rain gauge data of surface precipitation at Ogimi. On 25 July, rain was observed from 15:50-17:40 JST at the Ogimi radar site. The  $N^2$  at an altitude of 1.3 km was relatively large from 14:00-15:28 JST ( $2.06 \times 10^{-4} \text{ rad/s}^2$  at 15:24-15:28 JST), but it suddenly decreased to  $0.86 \times 10^{-4} \text{ rad/s}^2$  from 15:28-15:32 JST, and  $N^2$  increased afterward. It is interesting to note that small  $N^2$  values (a blue region in the figure) extended to higher altitude up to 2.0 km from 15:32-15:56 JST, and coincides with the on-set of the precipitation at 15:56 JST.

On 23 July we can also see a similar time-height structure for the low  $N^2$  in Fig. 7, which again appeared just before it started to rain. To provide more details on this, rain was observed from 13:40-14:45 JST with a peak (7 mm/10min) at 14:15 JST. However, only very weak rain (1 mm/10 min or less) was observed from 13:40-14:05 JST. The  $N^2$  at an altitude of 1.2 km (bottom of the observed height range) decreased from  $1.40 \times 10^{-4} \text{ rad/s}^2$  to  $0.40 \times 10^{-4} \text{ rad/s}^2$  during 13:28-13:40 JST. Unfortunately, the RASS temperature data were missing just before this drop in  $N^2$  (13:32-13:36 JST). From 13:40-13:44 JST,  $N^2$  was as small as  $0.40 \times 10^{-4} \text{ rad/s}^2$ . The region with the low static stability moved toward a higher altitude over time.

It is worth noting that a similar time-height structure for  $N^2$  was commonly seen on both 23 and 25 July, which coincided with the start of precipitation at the radar site. Therefore, both NHM model results and RASS observations suggest that decrease in the static stability, and its

further extension along altitude before precipitation are the two key factors for characterizing the development of a convective system.

#### 4. Convective Cells Inside A Meso- $\gamma$ -Scale Convective System

For a convective system on 23 July and 25 July, we first studied the behavior of temperature fluctuations accompanying with the passage of a convective system. We used  $T_v$  and wind velocity observed with WPR-RASS. For the case on 25 July we also employed the radar reflectivity observed by COBRA. We will discuss the relation between convective clouds and static stability, referring to the  $N^2$  structure described in Section 3.

##### 4.1 Details on Temperature Variations During Passage of Convective Cells

Figure 8 shows the horizontal distribution of radar reflectivity observed by COBRA from 15:48-16:00 JST and from 16:42-17:06 JST. At 15:12 JST, there was a convective system southeast of the Ogimi site. At 15:30 JST one convective cell was generated within the convective system, and it moved toward the west. Then, the convective system began to cover the Ogimi site, and more than two convective cells were generated inside the convective system. These cells moved west-northwest or west-southwest, but the convective system itself remained or moved slowly northwest, while generating a new cell in the northeast of the old cell. At 15:54 JST the convective cell passed over the Ogimi site (see the center-top panel in Fig. 8).

Although convective cells broke down and the convective system deteriorated at 16:18 JST, a new convective cell was generated again in the northwest of the Ogimi site at 16:24 JST, and this cell moved west-southwestward. Then more convective cells were generated in the convective

system, which moved west-southwest or southwest. However, the convective system itself again remained and generated a new cell northeast of the old cell. At 16:48 JST and from 17:00-17:12 JST, convective cells passed over the Ogimi radar site (see the center panel in the row and bottom panels in Fig. 8). At 17:36 JST, the convective system disappeared over the Ogimi site. Considering the motion of convective cells, we define the period until 16:18 JST as the first period, and the subsequent one as the second period.

Figure 9 shows the time height distribution for radar reflectivity over the Ogimi site composed from RHI scans of COBRA during the first period. The RHI scan started at 15:29 JST. Figure 9 indicates that a strong convective cell (with reflectivity above 55 dBZ) passed over the Ogimi site at around 15:54 JST. Although COBRA had a time resolution of about 6 minutes, the convective cell within the convective system moved faster than the time resolution of COBRA, and therefore they are not fully visible in Fig. 9. Instead, the development and decline of a convective system can be seen in Fig. 9.

Figure 10 (a) and (b) show the time height distribution of the perturbation of  $T_v$ , and the vertical wind velocity,  $w$ , from the WPR-RASS on 25 July, respectively. The blank region in Fig. 10 indicates the missing data. It is interesting to note that during the time when convection was active (see Fig. 9), large fluctuations of  $w$  with a short time scale are also seen (Fig. 10 b). Below about 2 km altitudes during 15:30-16:10 JST  $w$  was mostly upward, and became downward after 16:10-16:20 JST. Intense upward  $w$  sometimes appeared with the maximum amplitude of about 0.7 m/s, extending up to 3.1 km at 15:50 JST and 3.6 km at 16:10 JST, respectively. Direction of  $w$  alternated between upward and downward above about 2.5 km, which seems to be affected by a passage of convective cells. Positive increase of  $T_v$  was generally recognized within the convective

cells (see Fig. 9). In particular, the perturbations of  $T_v$  as large as 2.7 K were seen at 15:50-16:10 JST coinciding with large upward  $w$  (unfortunately,  $w$  is missing at around 16:05 JST). On the other hand, just below such  $T_v$  increase  $T_v$  within the cell sharply decreased at 1.8-2.0 km during 16:00-16:05 JST. Decrease in  $T_v$  was also seen from 16:10-16:20 JST after the convective cells passed over the Ogimi radar site.

These results suggest that  $T_v$  fluctuation were accompanied by a cycle of development and dissipation in the convective system. The increase of  $T_v$  inside the convective system can be caused by the release of latent heat during cloud generation.  $T_v$  inside the convective system decreased, because rain particles descended and evaporated near the cloud base, and the convective system seemed to deteriorate due to this cold air.

Figure 11 shows a time-height section of the vertical wind velocity from the NHM model at the location of a developed convective system (cross symbol in Fig. 3). CAPE in the NHM model was estimated to be 1202.4 J/kg. And, the maximum upward wind velocity in NHM was about 5 m/s at the level of 750-650 hPa, which is consistent with the largest limit (5.8 m/s) estimated from CAPE, while, the WPR-RASS observations in Fig. 10 showed the amplitudes of only up to about 1 m/s.

It is reasonable for the NHM model to show such intense upward winds near the core of a localized convective system, considering the grid size of 1 km. On the other hand, the center of a convective system did not seem to pass right overhead of WPR, which may reduce the maximum vertical wind velocity in the observations; with WPR observation it is generally difficult to detect the core of a convective cell with a horizontal scale of about 100m.

## 4.2 Relation Between Convective Clouds and the Atmospheric Static Stability

Here, we discuss the relation between convective clouds and atmospheric static stability, mainly referring to the case on 25 July. Figure 12 shows the time height distribution for  $N^2$ , where the solid line indicates a cross section of reflectivity observed by COBRA. We focused our attention on the time around 15:30 JST when the convective system during the first period began to develop. A weak echo with its peak at 1.8 km began to appear at 15:30 JST (see Fig. 9). At this time,  $T_v$  increased inside the weak echo that appeared over the Ogimi site (see Fig. 10). As the  $T_v$  inside the echo was high, and the atmosphere above the region had low  $T_v$ , the atmospheric static stability tended to decrease near the echo's top height.

The region with low static stability corresponded to the unique  $N^2$  structure in association with the generation of convection discussed in Section 3. We estimated the cloud water content (CWC) from the NHM model in Fig. 13, where the solid line indicates a cross section of clouds. We can clearly see that the cloud top height coincided with the low  $N^2$  region, which rapidly moved upward. That is, at 14:20 JST a cloud appeared at 1.1-1.2 km, then its top moved upward reaching an altitude higher than 4 km. Such a time-height structure agrees quite well with the low static stability structure shown in Fig. 13.

Before it started to rain, the time-height structure of the low  $N^2$  region asymptotically agreed with increase of the cloud top height. Decreases in static stability near a cloud top could be caused by the increase of  $T_v$  inside the cloud. The cloud further developed to reach higher altitudes because of unstable condition near the cloud top.

## 5. Generation Mechanism for a Convective Systems

We discuss the generation and development mechanism for a convective system on 23 and 25 July 2007, paying particular attention to the atmospheric temperature structure and sea breeze circulation.

## 5.1 Effects of atmospheric temperature structure on generation of a convective system

Figure 14 shows the height profiles of  $T_v$  perturbation and horizontal wind velocity with WPR-RASS from 10:30-12:30 JST on 25 July. The air with low  $T_v$  started to penetrate the atmosphere at 1.0-2.5 km. The meridional wind velocity,  $v$ , and  $T_v$  changed with a similar cycle. The air with low  $T_v$  seemed to flow from the southeast into this region where virtual temperature was low.

Figure 15 shows the time-height distribution for the perturbations of  $T_v$  and  $w$  on 25 July. Surface temperature  $T_s$  at Ogimi is also plotted in Fig. 15 (c).  $T_s$  started to increase at 06:00 after the sunrise. During 10:00-16:00 JST  $T_s$  showed short-term perturbations, but  $T_s$  did not decrease below the daily mean temperature (26.7°C). Then, a rapid decrease in  $T_s$  was seen after about 16:00 JST. Note that a rain was observed at the Ogimi site from 15:50-17:40 JST, as shown in Fig. 6.

Figure 15 (a) shows that  $T_v$  at 1.0-2.0 km gradually increased after 07:00 JST, which is generally consistent with the increase in  $T_s$ . However, after 10:00 JST  $T_v$  started to decrease in the lowest layer, and the region with negative  $T_v$  deviation with magnitude of about 0.4 K expanded toward higher altitudes. This  $T_v$  variation seems to be caused by an inflow of air with low  $T_v$ , which will be discussed in a later section by referring to NHM forecast results. It is noteworthy that a sharp  $T_v$  increase can be clearly recognized at about 16:00 JST, which is embedded in the colder  $T_v$  region.

Next, let us investigate the behavior of  $w$  in Fig.15 (b). In general,  $w$  abruptly fluctuated within short time scales. And, alternating up-/down-ward motions were more enhanced after 10:00 JST coinciding with the inflow of the air with low  $T_v$ . During 10:00-14:00 JST the upward winds were suppressed near the upper edge of the air with low  $T_v$ . After around 14:00 JST the  $w$  fluctuations became much stronger than those in the previous period, and they penetrated above the upper edge of the atmosphere with low  $T_v$ . The maximum amplitudes of  $w$  fluctuations ranged from -1.3 m/s to 0.8m/s.

According to the NHM model results, the water vapor mixing ratio at the surface became as high as 20 g/kg (20.2 - 21.2 g/kg) from 10:00-20:00 JST. This implies that a moist air with high temperature was formed near the ground. Therefore, after 10:00JST, the vertical gradient of  $T_v$  became negative in the height range between the ground and the 1.0-2.5 km region. This seems to have been caused by the inflow of air with low  $T_v$  into this region. Further, it suggests that stratification with low static stability was formed in this height range.

## 5.2 Sea Breeze Circulation

We referred to the NHM model results to study the effects of sea breeze circulation on a meso-scale convective system. In particular, we focussed on the case on 25 July. The topography of the island of Okinawa is basically flat in the region south of 26.5° N (see Fig. 2), and there are hills with an elevation of 250-350 m in the north. We selected a cross section passing through the Ogimi radar site, which is indicated as A-A' in Fig. 2 aligned nearly perpendicular to the island. Figure 16 show the wind velocity vector projected onto the cross section, and the contour indicates the convergence of horizontal wind in the cross section on 25 July. Note that only the deviation from

the time mean is plotted for the horizontal wind. The Ogimi site is located on the north-west side of a hill top as indicated by the dashed line in Fig. 16.

A sea breeze flowed into a surface layer from the neighboring sea on both sides of the island, and the sea breeze began earlier on the east coast from 10:00 JST (start of NHM simulation). After 11:00 JST, a sea breeze also started from the west coast, then convergence ( $-0.05$  /s) began in the lower layer. As the sea breeze on the west coast deeply penetrated inland, the convergence region moved toward the inland side. After 11:30 JST, because the sea breeze from both coasts collided over the land, convergence became larger ( $-0.08$ /s), and the vertical winds were also enhanced. When convergence reached its strongest as  $-0.17$  /s at 13:35 JST, the vertical wind amplitude became maximum and upward at  $0.67$  m/s. Therefore, the warm moist air in the lower layer was raised by this upward wind. This air mass then reached LCL (at about  $0.4$  km above the sea surface level), resulting in the generation of convective clouds.

### 5.3 Discussion on a Generation Mechanism

We summarize a plausible mechanism for the generation of the convective system based on the results presented in the earlier subsections. Figure 17 is a schematic of the generation mechanism for a convective system. First, there is humid air near the surface, which is clarified by referring to the NHM model. After sunrise, the ground surface is heated by solar insolation, and warm and moist atmosphere is formed near the surface ((i) in Fig. 17). The WPR-RASS observations revealed that an atmosphere with low  $T_v$  flowed into the layer at altitude of  $1.2$ - $2.5$  km or  $3.5$  km ((ii) in Fig. 17). As a result, a lower atmospheric layer (about  $1.2$  km or below) became unstable ((iii) in Fig. 17). The NHM model indicates that sea breeze circulation



occurred in this statically unstable layer. Note that sea breeze circulation occurred on both sides of the island. The convergence of the horizontal wind occurred in the lower layer due to the sea breeze. As the sea breeze began to deeply penetrate inland, the convergence region also moved inland. In the afternoon, the sea breeze from both coasts collided over the land, and the convergence increased ((iv) in Fig. 17). As convergence increased, vertical winds were also enhanced upward. When the vertical wind arises in a lower layer with low static stability, the high temperature and high humidity atmosphere near the ground is uplifted, which generates clouds ((v) in Fig. 17).

In order to investigate the influence of geographical feature on the generation mechanism of a convective system, we performed the NHM forecast for the case of 25 July in which topography and land-sea distribution of the surface temperature was modified from a realistic condition. By neglecting the topography (elevation of the island), but keeping contrast in the surface temperature between land and ocean, no significant changes occurred in generating convections. On the other hand, convections were not generated when the land temperature was set equal to the sea surface temperature in the surrounding sea. The model studies also suggest that the generation of convection is related to the day-night contrast, that is, convection was not generated under a night condition. It is important for the land surface to be sufficiently heated by solar radiation to generate convection.

Shafer et al. [2001] investigated the boundary layer development in the tropics from MCTEX conducted over Melville Islands in Northern Australia. They showed that the boundary layer grew rapidly due to the land surface heating in the morning, and the boundary layer top reached to 1.5 km by early afternoon. The sea breeze circulations increased with its maximum convergence at 12:00 in local time. Thunderstorms firstly developed on the east coast where the sea

breeze opposes the local environmental flow. Then, thunderstorm outflows stabilized the boundary layer, and the convergence by the sea breeze was replaced by the divergent flow because of the outflow of thunderstorm.

Our results were basically consistent with Shafer et al. [2001] in that the sea breeze circulation is a key factor to develop the convection. However, there also exist some differences. First, development of the boundary layer was not clearly recognized in our analysis, but advection of the air with low virtual temperature from the ocean played an important role to generate low static stability. The convergence due to the sea breeze circulations appeared in the center of the Okinawa Island, although the thunderstorms developed on the east coast during MCTEX. Stabilizing effects of the thunderstorm outflows were not clearly recognized in our analysis, probably because the convective activity did not develop to an intense thunderstorm.

Although the large scale suppressed environment due to a Pacific high-pressure was in general similar to the build up phase for island thunderstorms during the prelude to the monsoon in the northern Australia [May and Ballinger, 2007], deep convective storms did not appear over Okinawa. But, a convective system with a relatively low cloud top height was dominant around Okinawa, and lightning and hail storms are rare. These were also observed during an intensive campaign of the Baiu front with COBRA [Shusse et al., 2009].

## 6. Conclusions

We studied the generation and development of a meso- $\gamma$ -scale convective system observed over the island of Okinawa when the area was covered with a Pacific high-pressure system in summer. Using detailed temperature profiles with high temporal and vertical resolutions obtained

from 443MHz WPR-RASS measurements, we analyzed two cases of the convective systems on 23 and 25 July 2007 that passed over the Ogimi radar site.

We first evaluated synoptic background conditions in terms of atmospheric stability using 12-hourly routine balloon observations at the Naha weather station from 21-26 July. In the lower layer below about 0.5–1 km,  $\theta_e$  was higher than 350 K, consisting of a warm and moist air over the whole period. At 2.5-5 km, as  $\theta_e$  was small (<334 K), the region below was convectively unstable. Before it rained on 23 and 25 July, CAPE was as large as about 1200-1250 J/kg, and CIN was small (about 2-3 J/kg), so convections could easily be generated. The operational weather radar results indicated strong convective clouds with a typical horizontal scale of 10 km and temporal scale of 40 - 60 minutes, respectively. Many convective systems were generated from 11:00-18:00 JST over the island of Okinawa.

We analyzed the Brunt-Vaisala frequency squared,  $N^2$ , with a time resolution of four minutes using the virtual temperature  $T_v$  profiles observed by 443MHz WPR-RASS, and investigated what effects the atmospheric stability structure had on the generation and development of a convective system. Just before it rained on 23 and 25 July, a small  $N^2$  region extended toward higher altitude up to 2.0 km. The NHM model results also suggest that there is an important relation between the  $N^2$  structure and the development of a convective system.

We discussed the temperature and vertical wind fluctuations accompanying the passage of a convective system on 25 July, also employing the COBRA data. An increase of  $T_v$  was seen in region with abrupt vertical wind fluctuations, and this was mostly associated with upward winds, and a decrease of  $T_v$  was seen during downward winds. The  $T_v$  fluctuations were accompanied by a cycle of development and dissipation of the convective system.

Before it started to rain, the time-height structure of the low  $N^2$  region asymptotically agreed with the increase in the cloud top height. We investigated the cloud water content (CWC) from the NHM model to examine the general relation between the structure of static stability and clouds. Decreases in the static stability near the cloud top seemed to be caused by the increase of  $T_v$  inside clouds. Clouds further developed higher because of unstable condition near the cloud top.

On the basis of observational studies, we proposed a generation and development mechanism for a convective system as follows: 1) there is moist air near the ground, and as the surface temperature increases due to solar radiation, a warm and moist layer is formed. 2) When an atmosphere with low  $T_v$  flows into the upper layer (about 1 - 3 km) the static stability of the lower layer decreases. 3) The sea breeze from both coasts collides over land, and convergence increases enhancing vertical winds, which develop convective clouds.

Both the 443 MHz WPR-RASS observations and NHM model results suggest that the time-height structure of atmospheric stability is important in the generation and development of a convective system. The inflow of air with low  $T_v$  at altitude of 1-3 km as well as the increase in temperature by solar radiation in the surface layer were important for generating a convective system. Although the background conditions looked similar during 21-26 July at the Ogimi radar site, the convective system was not necessarily generated, but significant events only occurred on 25 and 23 July. We found that the inflow of air with low  $T_v$  into the island area is a key factor in triggering a convective system. That is, unstable condition can easily be generated when the air with low  $T_v$  lies over heated air near the surface. Our case studies suggest that this unstable condition should coincide with the convergence of horizontal winds due to sea breeze.

## Acknowledgements

The 443MHz WPR-RASS and COBRA were operated by NICT. The RASS observations were conducted as a collaborative project between RISH and NICT. The study was partially supported by grants-in-aid for scientific research 18340140 and 17340142. We would like to thank Y. Shusse and M. Satake of NICT for providing us with the COBRA data sets. The intensive support and valuable suggestions provided by K. Saito of MRI and T. Iguchi of NICT are gratefully acknowledged.

## References

- Adachi, T., Development of a 400 MHz-band wind profiler radar with RASS, J. Commun. Res. Lab., 49, 211-216, 2002.
- Akaeda, K., T. Yokoyama, A. Tabata, M. Ishihara, and H. Sakakibara, Evolution of kinematic structure within a meso- $\beta$ -scale convective system in the growing and mature stages, Mon. Wea. Rev., 119, 2664-2676, 1991.
- Atkins, N.T., and R.M. Wakimoto, Observations of the sea-breeze front during CaPE. Part I, Dual-Doppler and aircraft analysis, Mon. Wea. Rev., 123, 944-969, 1995.
- Carbone, R. E., J. W. Wilson, T. D. Keenan, and J. M. Hacker, Tropical island convection in the absence of significant topography. Part I: Life cycle of diurnally forced convection, Mon. Wea. Rev., 128, 3459-3480, 2000.
- Chang, C.Y., and M. Yoshizaki, Numerical study of the mesoscale convective system observed over the Okinawa island in June 1987, Mon. Wea. Rev., 119, 2724-2733, 1991.
- Emanuel, K.A, Atmospheric Convection, Oxford Press, 165-191, 1994.
- Keenan, T., P. May, G. Holland, S. Rutledge, R. Carbone, J. Wilson, M. Moncrieff, A. Crook, T. Takahashi, N. Tapper, M. Platt, J. Hacker, S. Sekelsky, K. Saito, K. Gage, The Maritime Continent Thunderstorm Experiment (MCTEX): Overview and some results. Bull. Amer. Meteor. Soc., 81, 2433-2455, 2000.
- Kobayashi, M., H. Hirano, S. Okada, T. Yamada, and M. Shimura, The Observation of Diurnal Variation of Wind in Spring over Urban Area of Tokyo, Proc. National Symposium on Wind Engineering., 18, 11-16, 2004.

- 1
- 2
- 3
- 4
- 5
- 6
- 7 Martner, B.E., D.B. Wuertz, B.B. Stankov, R.G. Strauch, E.R. Westwater, K.S. Gage, W.L. Ecklund,
- 8
- 9 C.L. Martin, and W. F. Dabberdt, An Evaluation of Wind Profiler, RASS, and Microwave
- 10
- 11 Radiometer Performance, Bul. Amer. Meteorol. Soc., 74: 599-613, 1993.
- 12
- 13
- 14 Matuura, N., Y. Masuda, H. Inuki, S. Kato, S. Fukao, T. Sato, and T. Tsuda, Radio acoustic
- 15
- 16 measurement of temperature profile in the troposphere and stratosphere. Nature, 323,
- 17
- 18 426-428, 1986.
- 19
- 20
- 21 May, P.T., Thermodynamic and Vertical Velocity Structure of Two Gust Fronts Observed with a
- 22
- 23 Wind Profiler/RASS during MCTEX, Mon. Wea. Rev., 127, 1796-1807, 1999.
- 24
- 25
- 26 May, P.T., and A. Ballinger, The Statistical Characteristics of Convective Cells in a Monsoon
- 27
- 28 Regime (Darwin, Northern Australia), Mon. Wea. Rev., 135, 82-93, 2007.
- 29
- 30
- 31 Nakagawa, K., H. Hanado, S. Satoh, and T. Iguchi, Development of the CRL Okinawa bistatic
- 32
- 33 polarimetric radar, J. Commun. Res. Lab., 49, 225-232, 2002.
- 34
- 35
- 36 Nakagawa, K., H. Hanado, S. Satoh, N. Takahashi, T. Iguchi, and K. Fukutani, Development of a
- 37
- 38 new C-band bistatic polarimetric radar and observation of typhoon events. Proc. 31st Conf.
- 39
- 40 on Radar Meteor., Seattle, Amer. Meteor. Soc., 863-866, 2003.
- 41
- 42
- 43 Nicholls, M.E., R.A. Pielke, and W.R. Cotton, A two-dimensional numerical investigation of the
- 44
- 45 interaction between sea breeze and deep convection over the Florida peninsula, Mon. Wea.
- 46
- 47 Rev, 119, 298-323, 1991.
- 48
- 49
- 50 Ninomiya, K., and T. Akiyama, Multi-scale features of Baiu, the summer monsoon over Japan and
- 51
- 52 the East Asia, J. Meteor. Sos. Jpn., 70, No.1B 467-495, 1992.
- 53
- 54
- 55 Pielke, R.A., A three-dimensional numerical model of the sea breezes over south Florida, Mon.
- 56
- 57 Wea. Rev., 102, 115-139, 1974.
- 58
- 59
- 60
- 61
- 62
- 63
- 64
- 65

- 1
- 2
- 3
- 4
- 5
- 6
- 7 Pielke, R.A., The predictability of sea-breeze generated thunderstorms, *Atmosfera*, 4, 65-78, 1991.
- 8
- 9 Schafer, R., P.T. May, T.D. Keenan, K. McGuffie, W.L. Ecklund, P.E. Johnston, K.S. Gage,
- 10
- 11 Boundary Layer Development over a Tropical Island during the Maritime Continent
- 12
- 13 Thunderstorm Experiment, *J. Atmos. Sci.*, 58, 2163-2179, 2001.
- 14
- 15
- 16 Saito, K., T. Fujita, Y. Yamada, J. Ishida, Y. Kumagai, K. Aranami, S. Ohmori, R. Nagasawa, S.
- 17
- 18 Kumagai, C. Muroi, T. Kato, H. Eito and Y. Yamazaki, The operational JMA
- 19
- 20 Nonhydrostatic Mesoscale Model. *Mon. Wea. Rev.*, 134, 1266-1298, 2006.
- 21
- 22
- 23 Shusse, Y., K. Nakagawa, N. Takahashi, S. Satoh, and T. Iguchi, Characteristics of polarimetric
- 24
- 25 radar variables in three types of rainfalls in a Baiu front event over the East China sea, *J.*
- 26
- 27 *Meteor. Soc. Japan*, 87, 865-875, 2009.
- 28
- 29
- 30 Tri W. Hadi, T. Horinouchi, T. Tsuda, H Hashiguchi, and S.Fukao, See-Breeze Circulation over
- 31
- 32 Jakarta, Indonesia: A Climatology Based on Boundary Layer Radar Observations, *Mon.*
- 33
- 34 *Wea. Rev.*, 130, 2153-2166, 2001.
- 35
- 36
- 37 Wakimoto, R.M., and N.T. Atkins, Observations of the see-breeze front during CaPE. Part I:
- 38
- 39 Single-Doppler, satellite, and cloud photogrammetry analysis, *Mon. Wea. Rev.*, 122,
- 40
- 41 1092-1114, 1994.
- 42
- 43
- 44 Wilson, J. W., R.E. Carbone, J.D. Tuttle, and T.D. Keenan, Tropical Island Convection in the
- 45
- 46 Absence of Significant Topography. Part II: Nowcasting Storm Evolution, *Mon. Wea. Rev.*,
- 47
- 48 129, 1637-1655, 2001.
- 49
- 50
- 51
- 52
- 53
- 54
- 55
- 56
- 57
- 58
- 59
- 60
- 61
- 62
- 63
- 64
- 65



## Figure captions

Fig.1 Time-height cross section of equivalent potential temperature  $\theta_e$  observed at Naha from 21-26 July 2007. Contour lines are drawn every 6 K. In light shaded areas  $\theta_e$  is less than 334K and in dark shaded area it is greater than 350K. A larger tic mark corresponds to the beginning of the day in local time (JST).

Fig. 2 Precipitation rate from an operational weather radar by JMA on 25 July 2007. Asterisk and triangle indicate location of the Ogimi observatory and Naha, respectively. Line (A-A') on the top left panel corresponds to a cross-section used in Fig. 16.

Fig. 3 Rainfall intensity (mm/hr) from the NHM forecast. A cross symbol in the panel indicates the grid point that is referred to in Figs. 4 and 11.

Fig. 4 Time-height cross section (top panel) of Brunt-Vaisala frequency squared,  $N^2$ , on 25 July 2007 calculated from NHM forecast at the location (cross symbol in Fig. 3) where convective system appeared. Bottom panel shows surface precipitation rate every 10 minutes.

Fig. 5 Same as Fig.4 except for the location without convective system.

Fig. 6 Time-height cross section of the virtual potential temperature (top panel), Brunt-Vaisala frequency squared,  $N^2$  (middle panel), on 25 July 2007 calculated from 443MHz WPR-RASS observations, and surface precipitation rate every 10 minutes at the radar site (bottom panel).

Fig. 7 Same as Fig. 6 except for results on 23 July 2007.

Fig. 8 Horizontal distribution of reflectivity at the 1.5 km altitude observed by COBRA from 15:48 (top left) to 17:12 JST (bottom right) on 25 July 2007. Cross symbol indicates the Ogimi WPR observatory.

Fig. 9 Time-height cross section of reflectivity over the Ogimi site observed by COBRA from 15:29-16:18 JST on 25 July 2007.

Fig. 10 Time-height cross section of (a)  $T_v$  perturbations and (b) vertical wind velocity from 15:00-16:30 JST observed with 443MHz WPR-RASS on 25 July 2007.

Fig. 11 Time-height distribution of the vertical wind velocity from NHM forecast at the cross symbol in Fig. 3.

Fig. 12 Time-height cross section of  $N^2$  on 25 July 2007 calculated from RASS data. Contour lines indicate radar reflectivity over the Ogimi radar site observed by COBRA from 15:29-16:18 JST with contour interval of 2 dBZ.

Fig. 13 A time-height cross section of  $N^2$  calculated from NHM data at the location of a convective system on 25 July 2007. Contour lines indicate CWC with a contour interval of  $0.5 \text{ g/m}^3$ .

Fig. 14 Height profiles of perturbation component of  $T_v$ , and zonal and meridional wind velocity from WPR observations on 25 July 2007. Data were averaged from 10:30 JST to 12:30 JST when air with low  $T_v$  started to penetrate inland at 1.0-2.5km.

Fig. 15 A time-height distribution of (a) perturbation of  $T_v$ , (b) vertical wind velocity from WPR observations, and (c) surface temperature at the Ogimi site on 25 July 2007.

Fig. 16 Wind vector and convergence of horizontal winds from NHM data on 25 July on the cross section orthogonal to island topography around Ogimi (a vertical dashed line). Panels (a) –

(d) corresponds to the results at 10:25, 11:05, 11:35 and 13:35 JST on 25 July 2007, respectively. Vector shows wind velocity projected onto cross section, and contour indicates divergence/convergence (positive for divergence) of horizontal wind.

Fig.17 Schematic of generation mechanism for convective system.

Equivalent potential temperature (K) at Naha

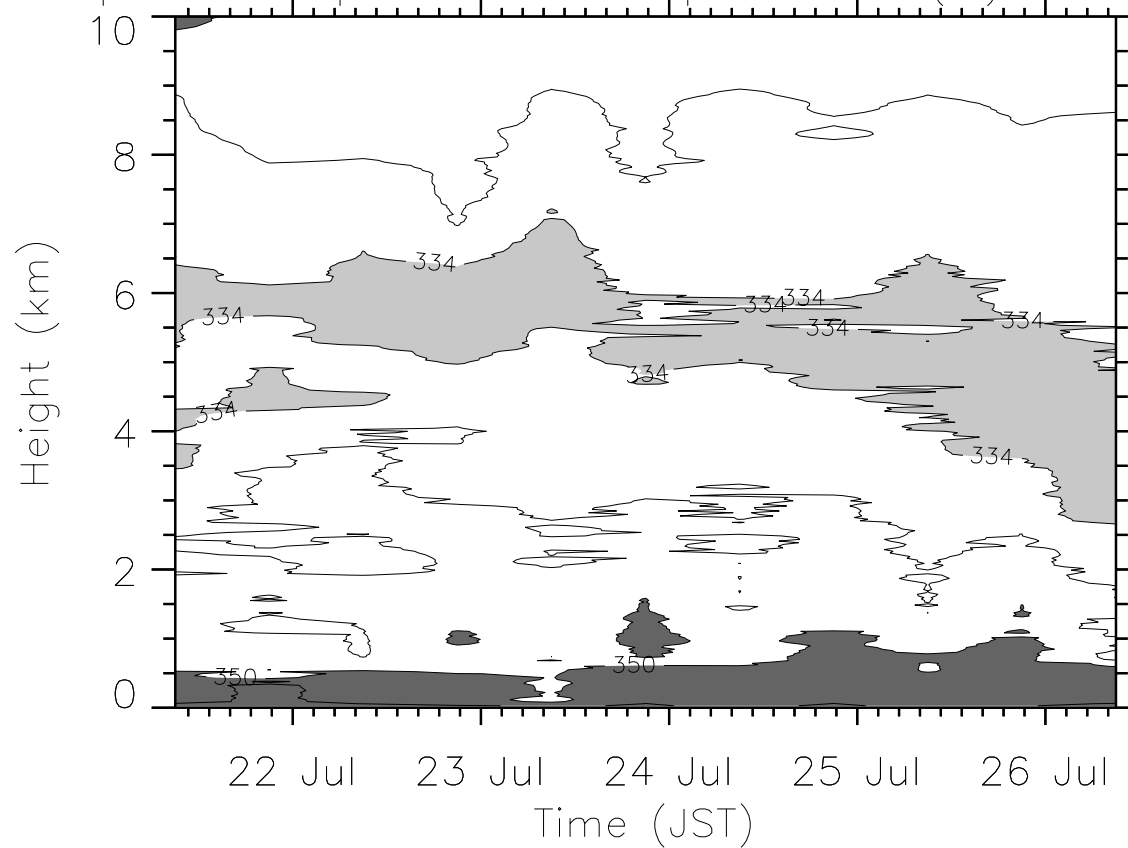


Figure 2

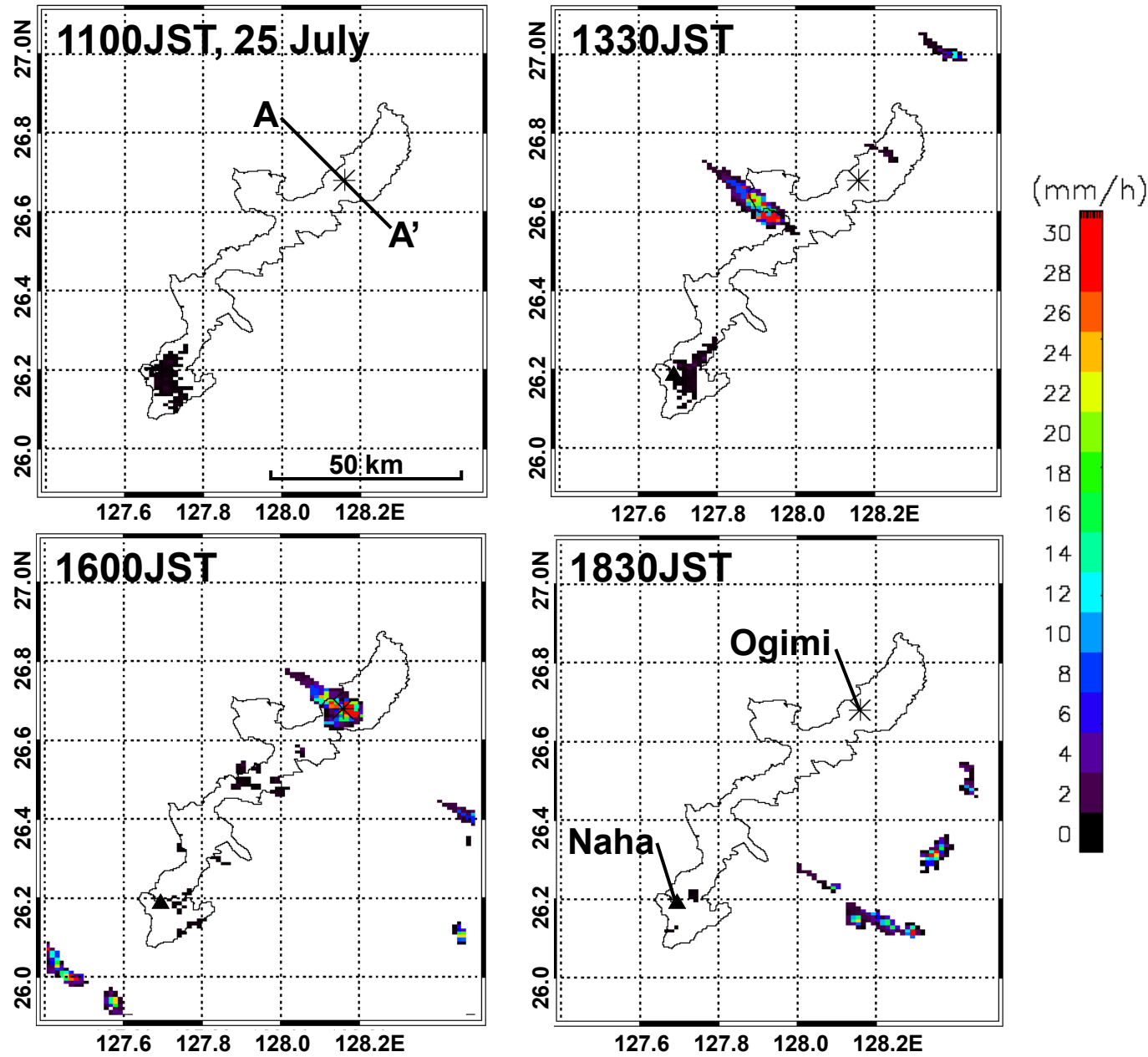


Figure 3

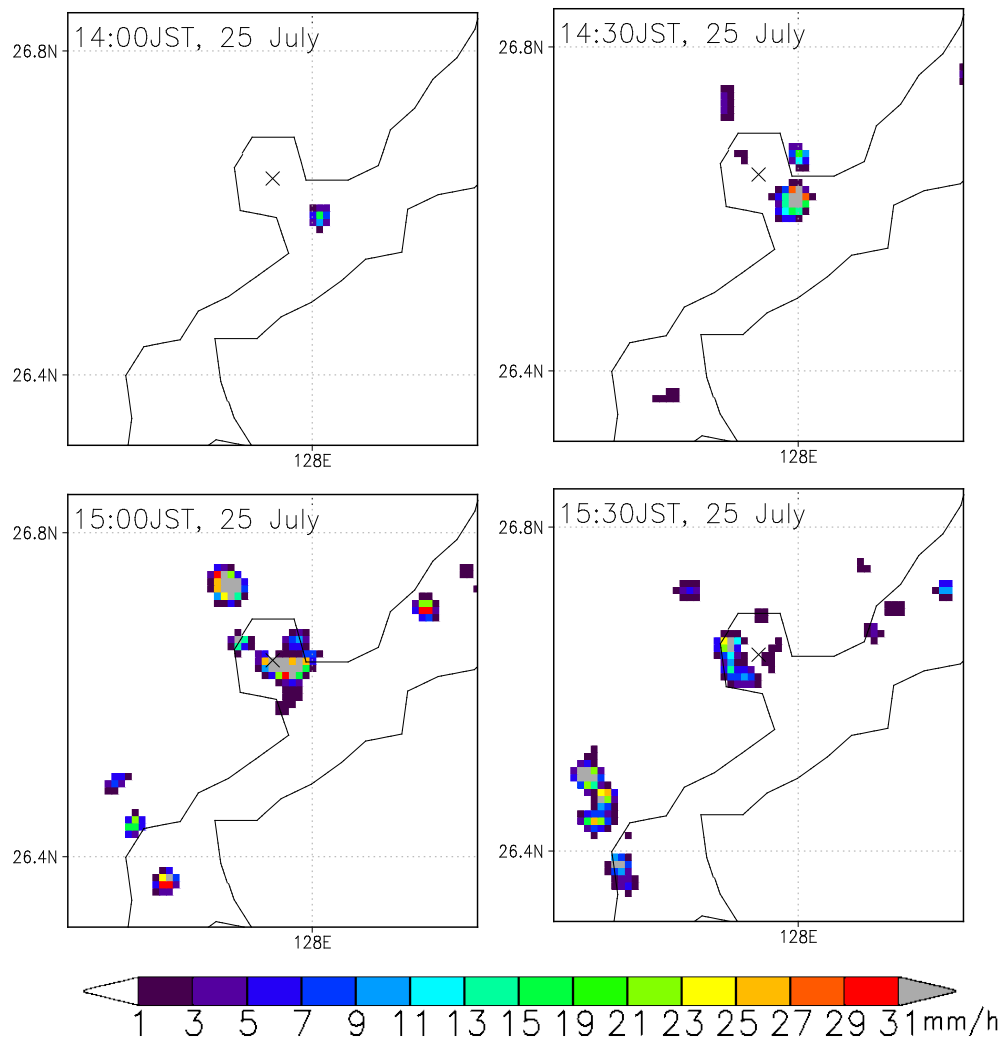


Figure 4

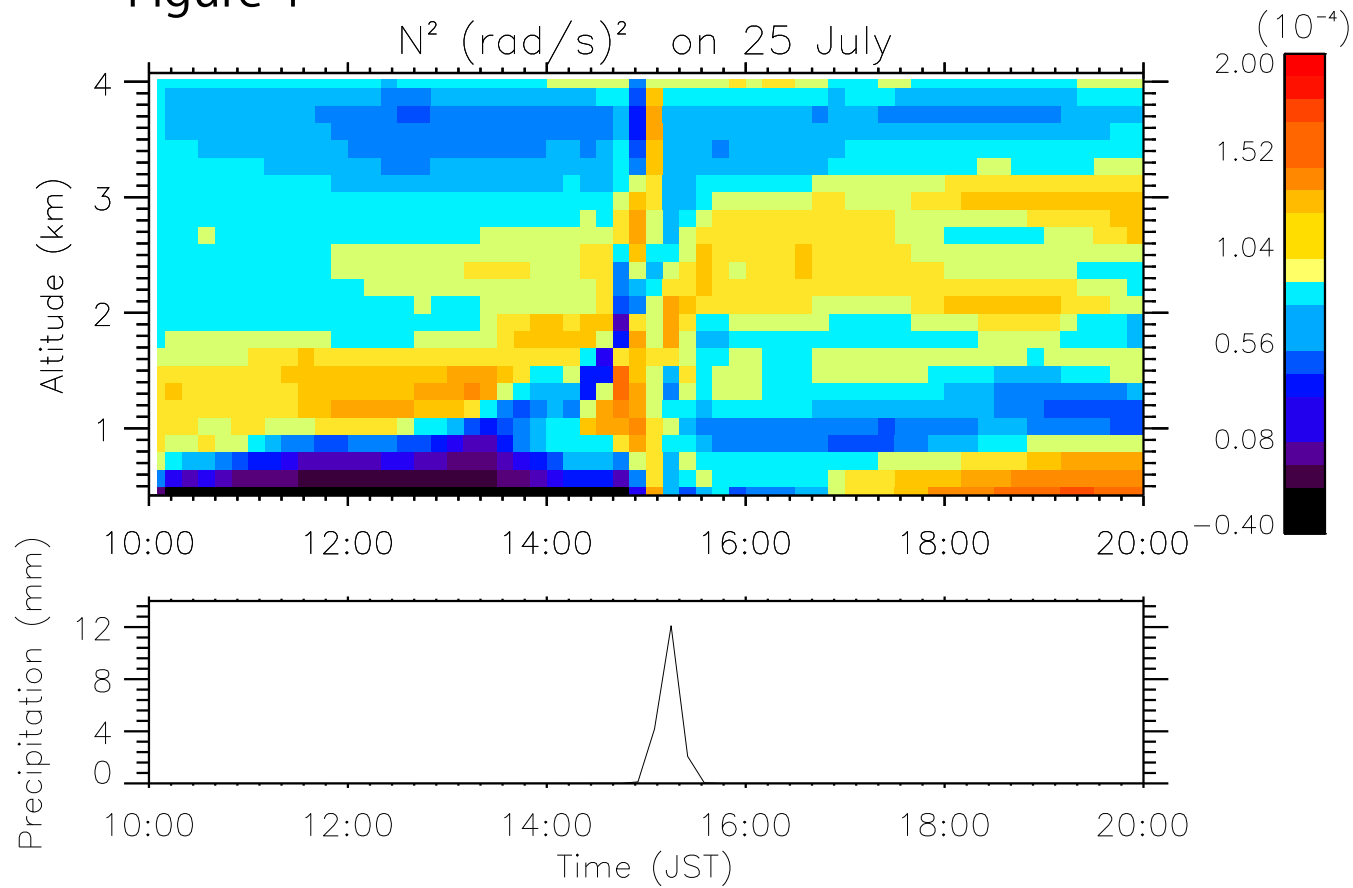


Figure 5

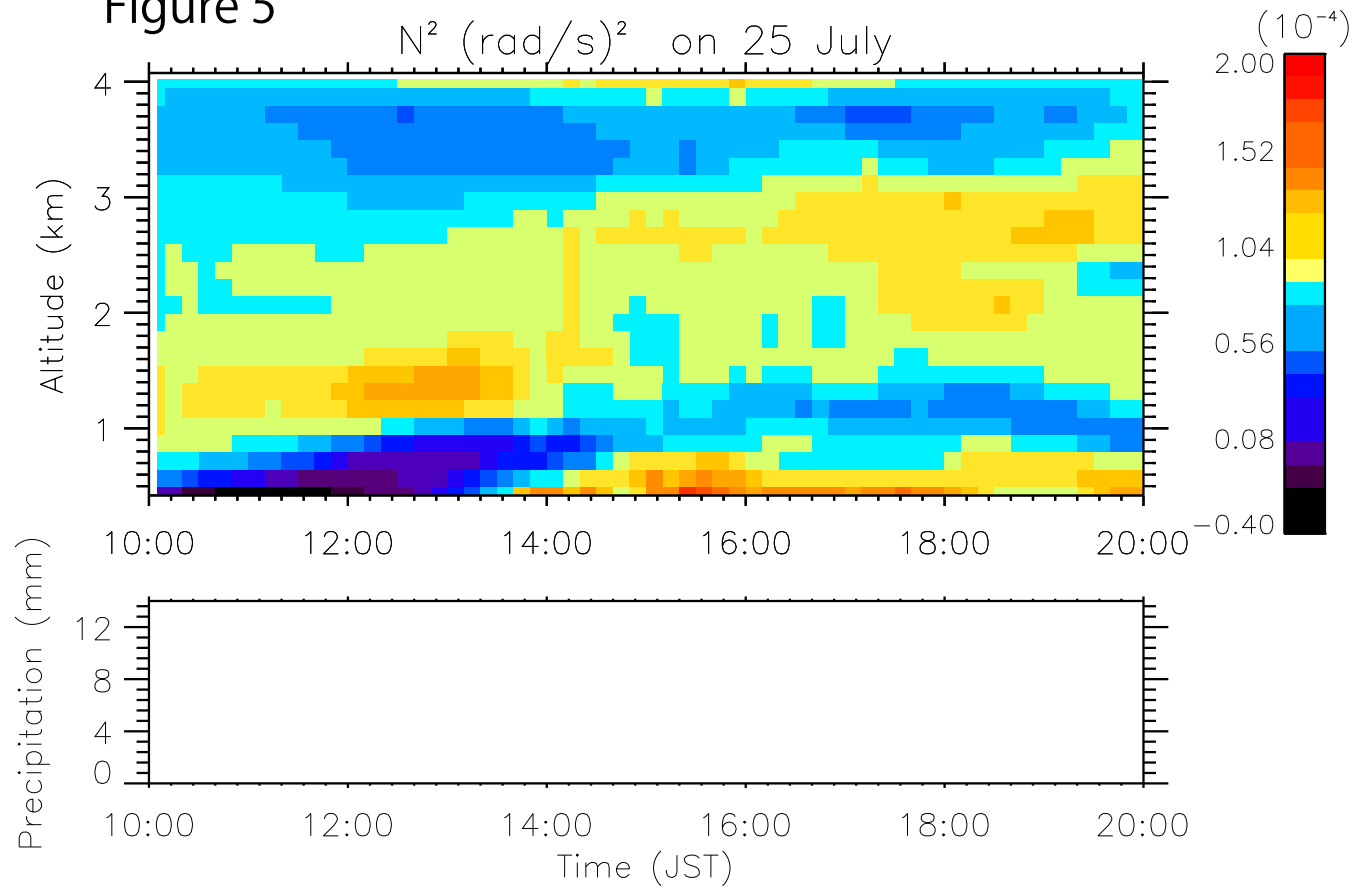




Figure 6

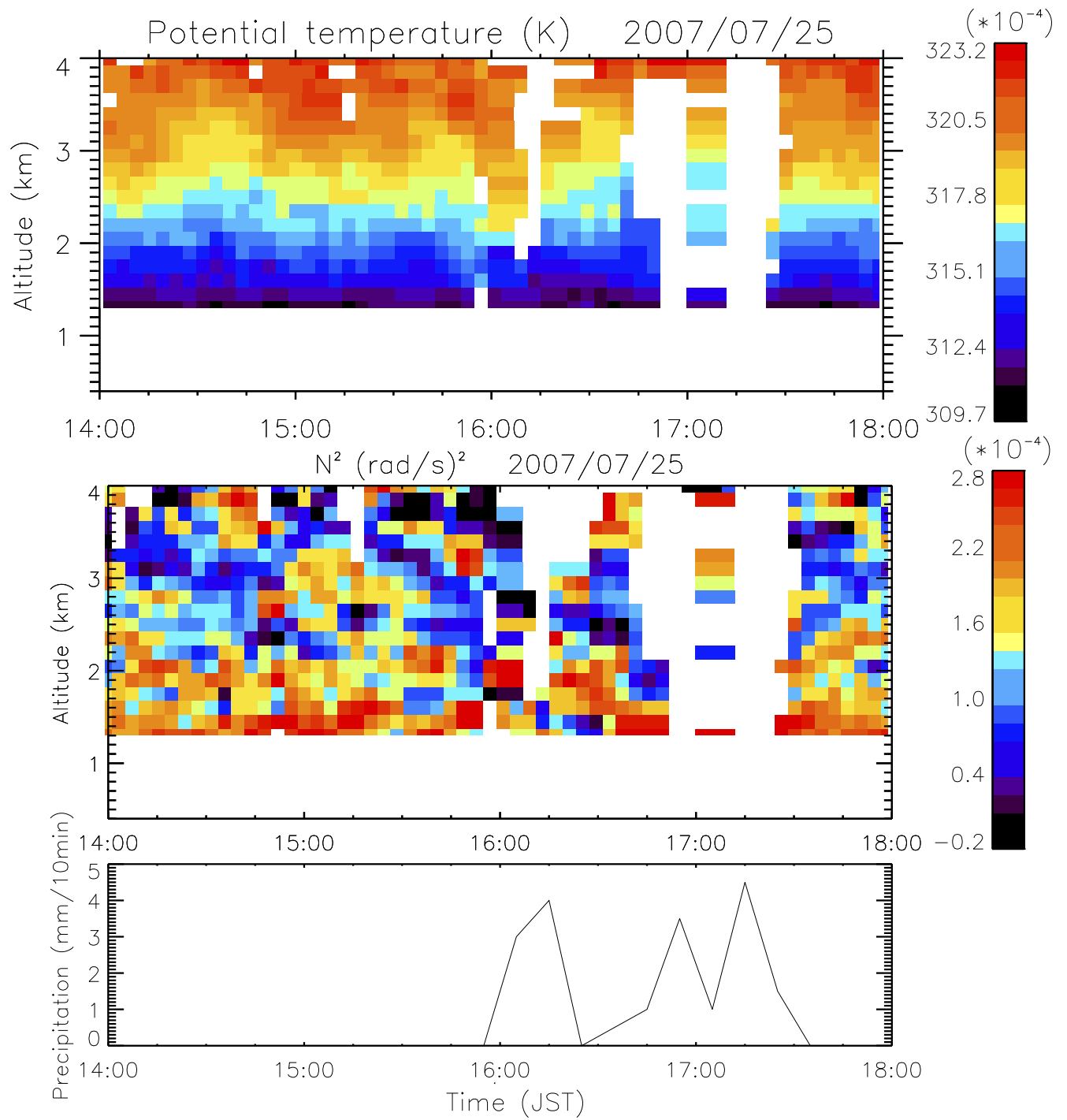


Figure 7

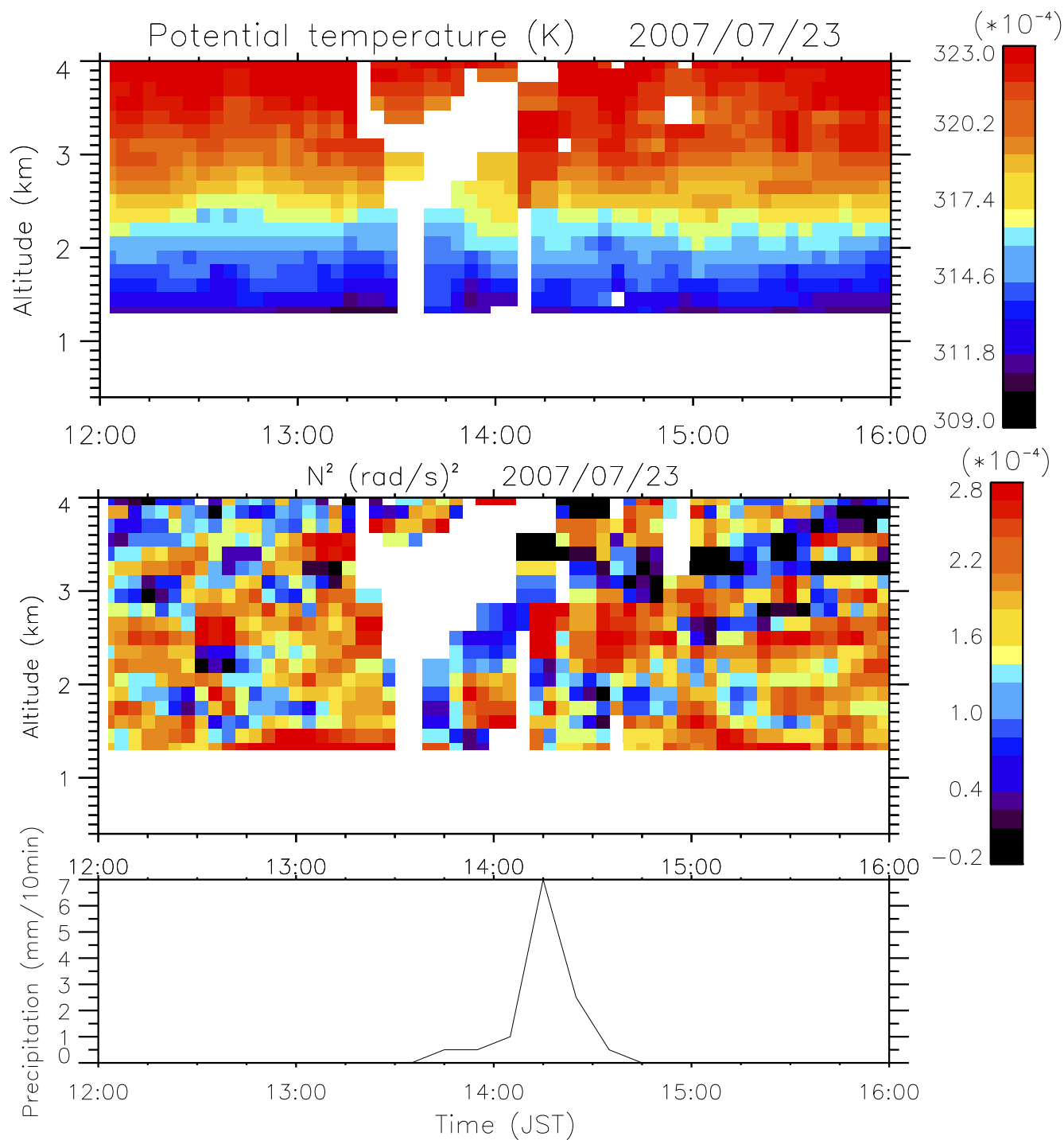


Figure 8

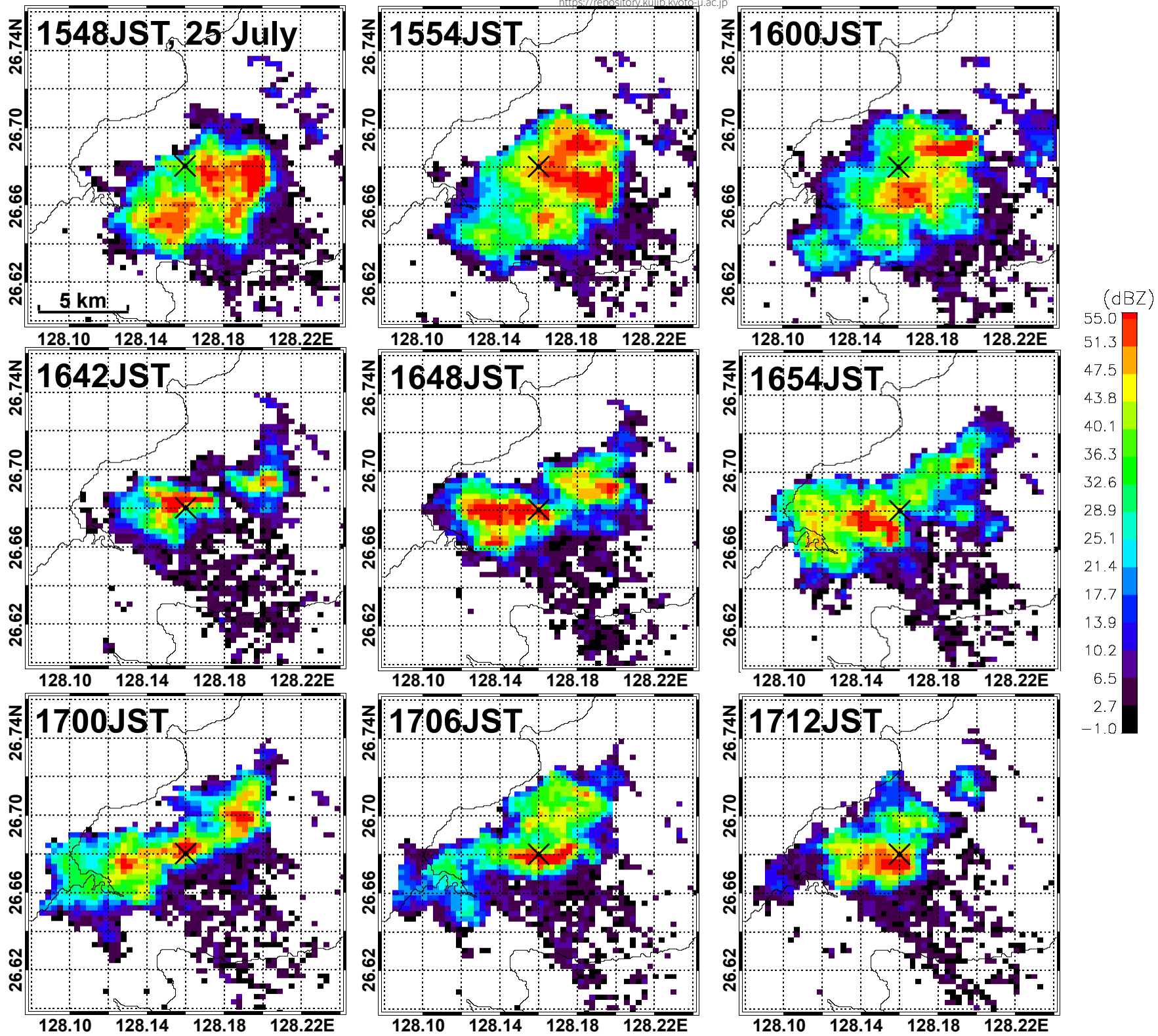


Figure 9

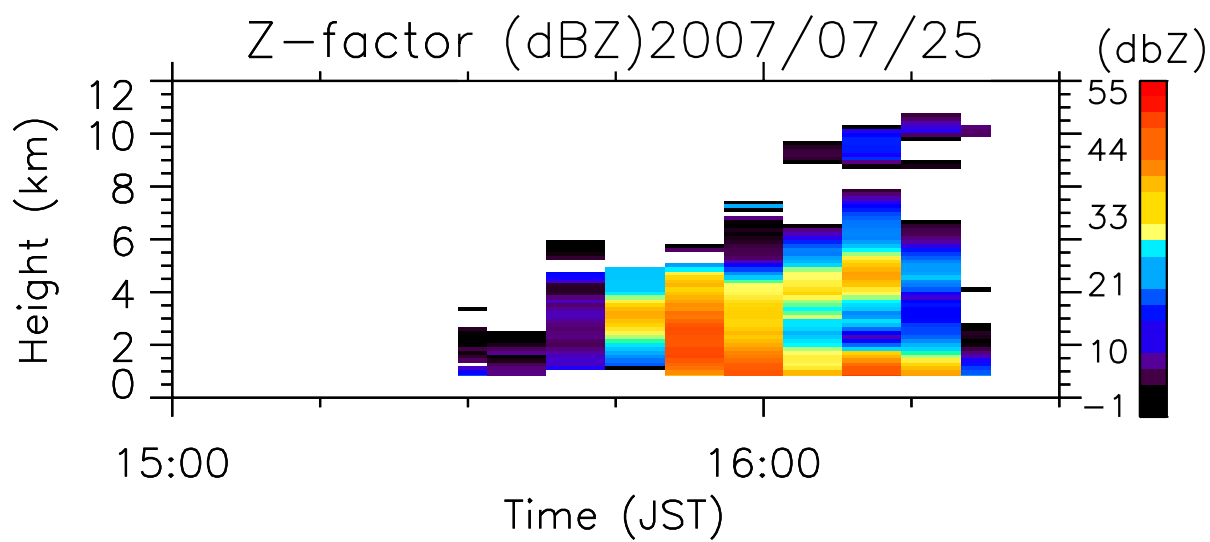


Figure 10

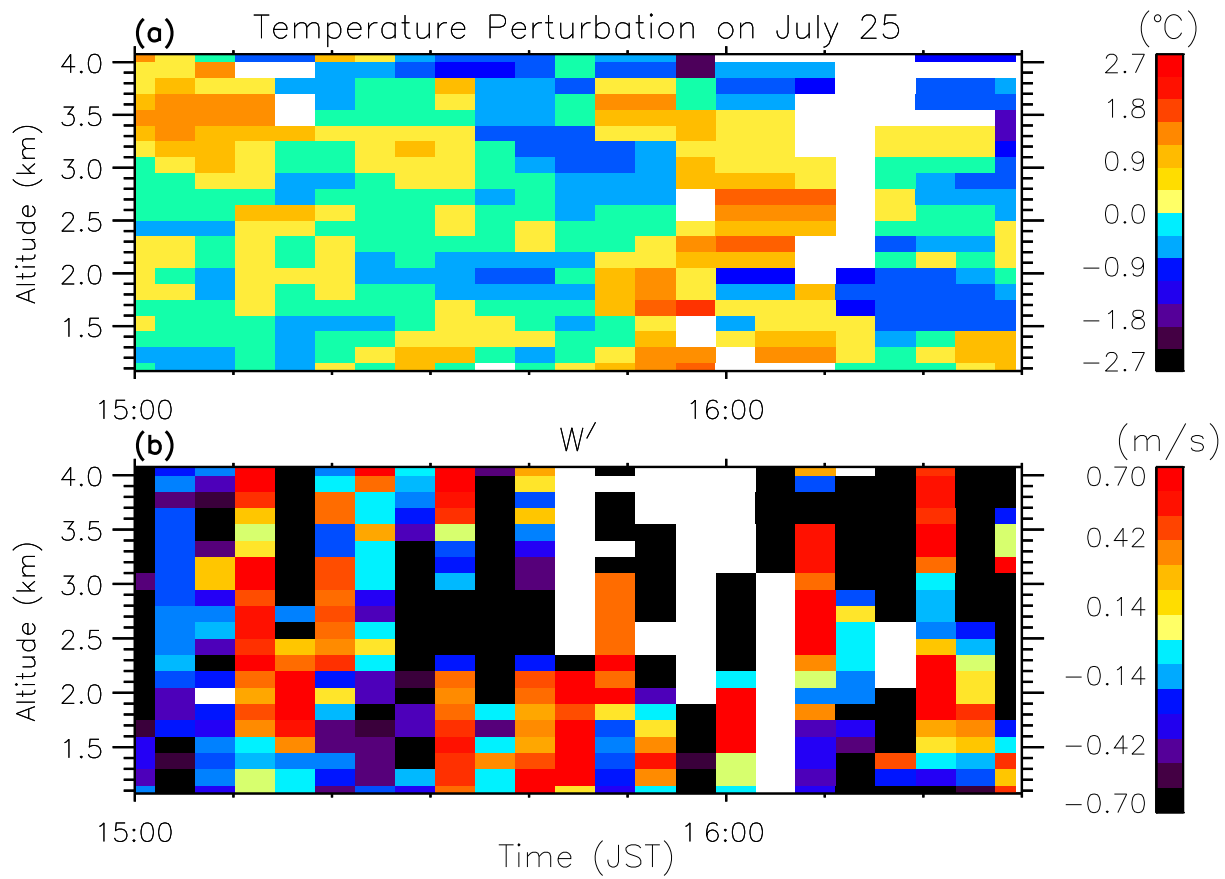
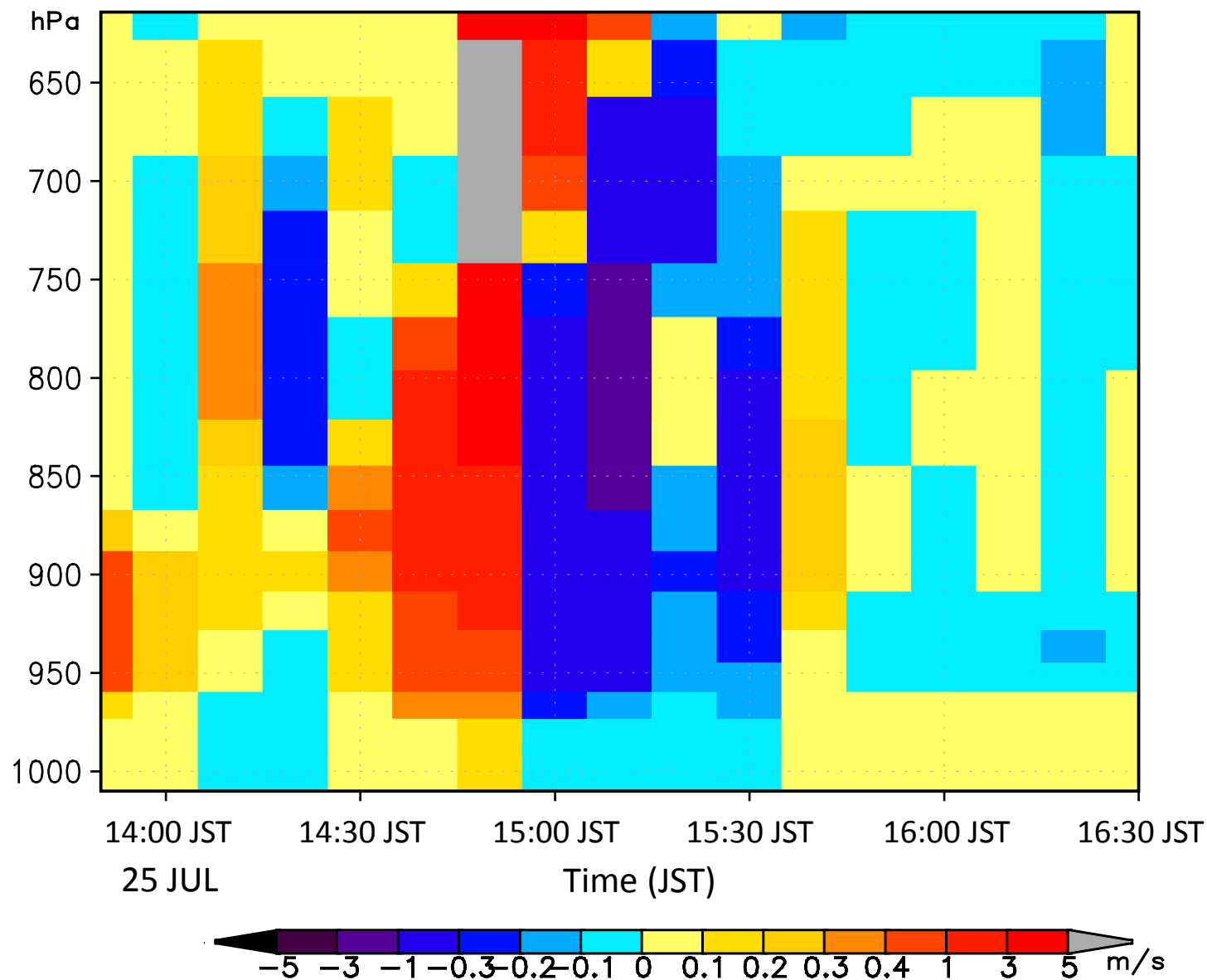
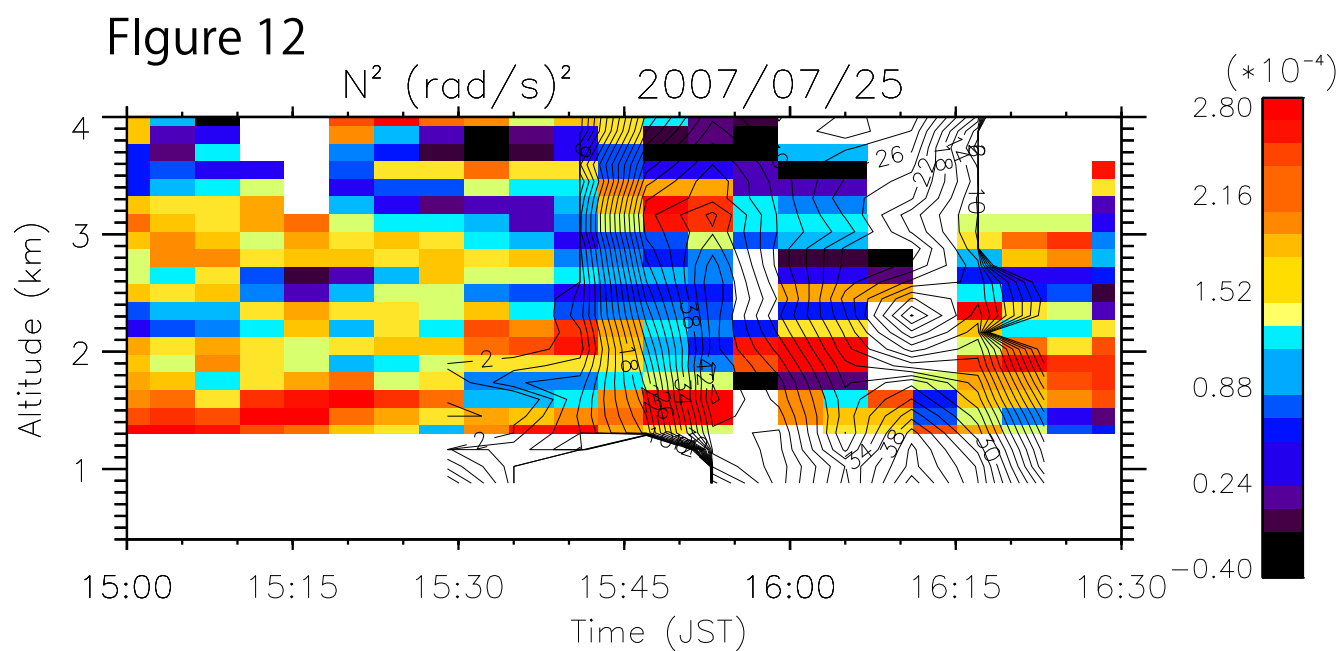
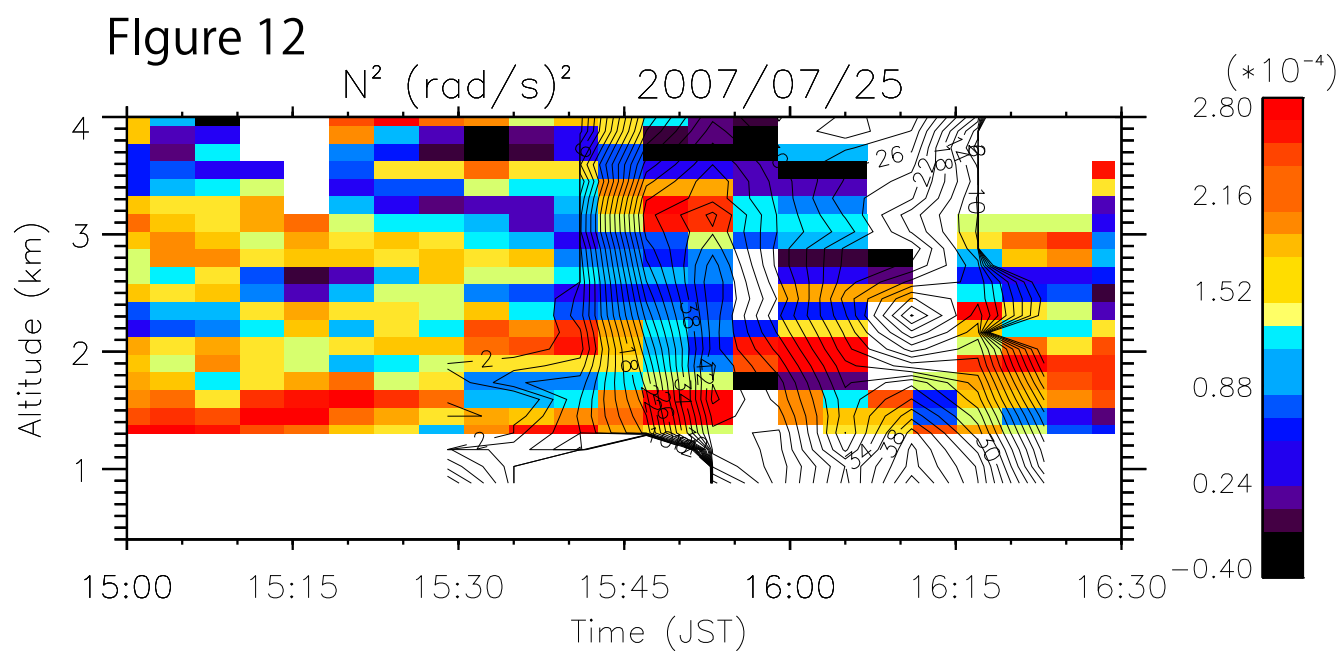


Figure 11









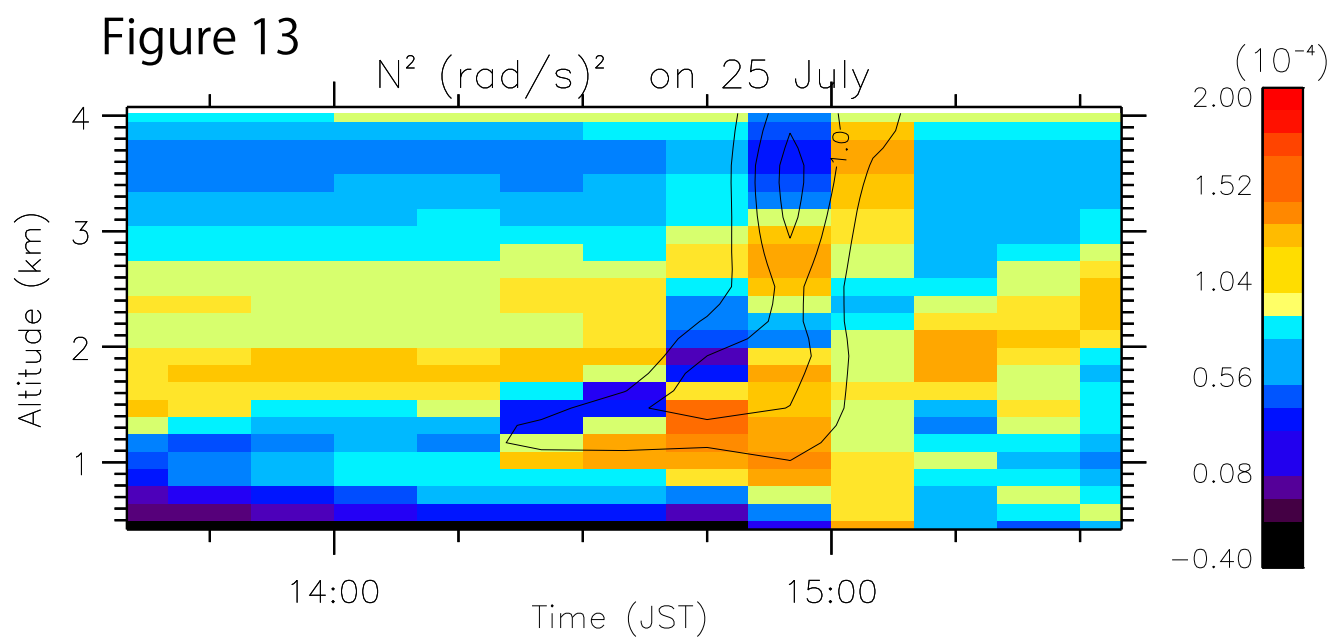


Figure 14

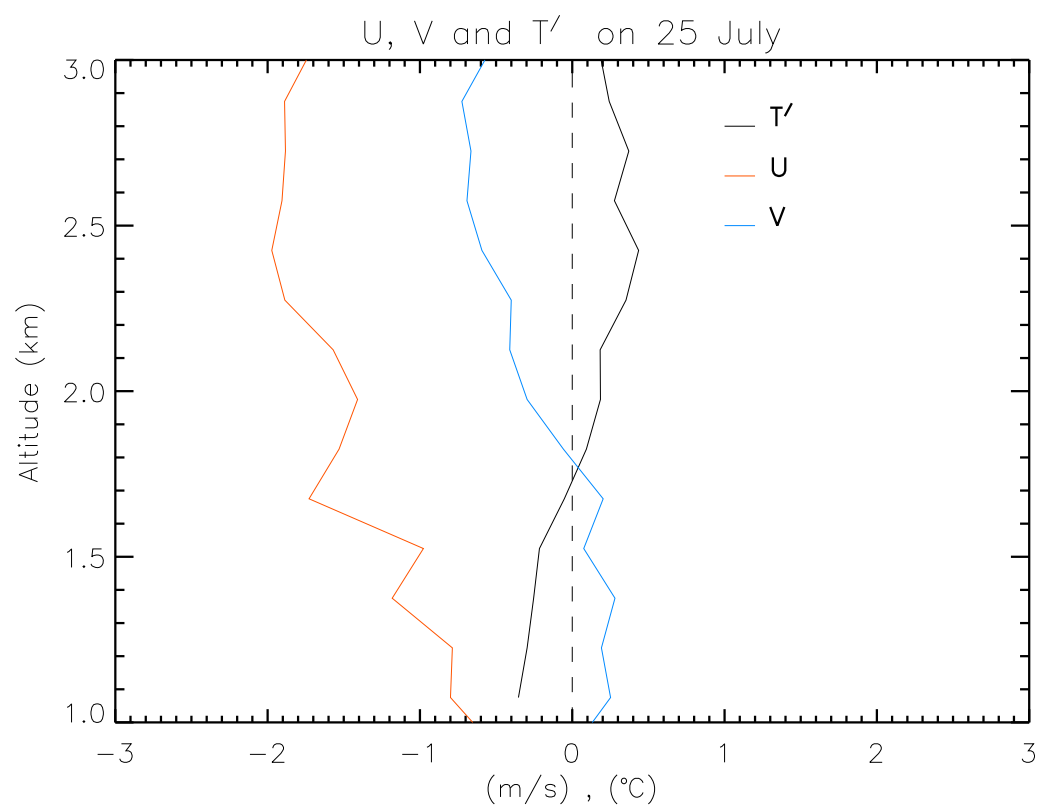


Figure 15

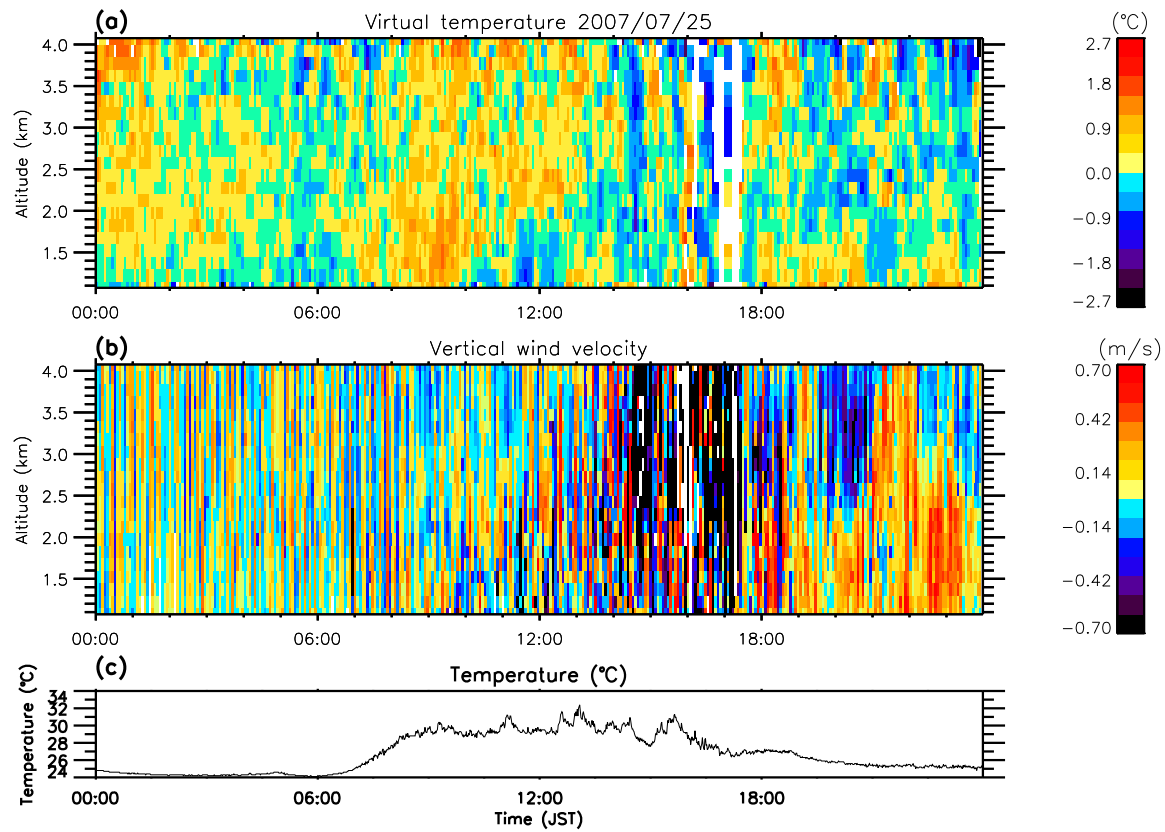


Figure 16

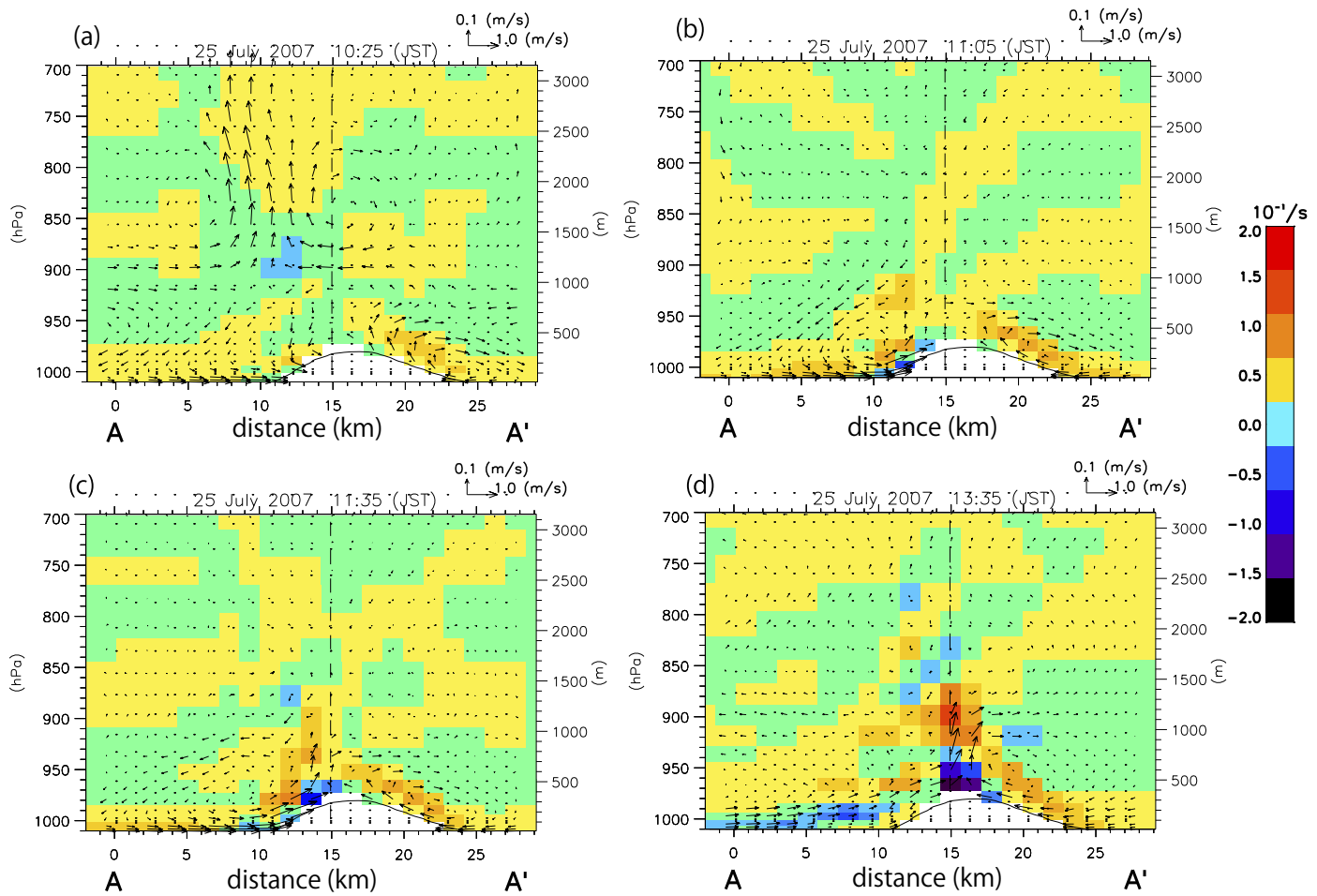


Figure 17

